Exciton localization-delocalization transition in an extended dendrimer

Vincent Pouthier*
Institut UTINAM, Université de Franche-Comté,
CNRS UMR 6213, 25030 Besançon Cedex, France
(Dated: December 2, 2013)

Exciton-mediated quantum state transfer between the periphery and the core of an extended dendrimer is investigated numerically. By mapping the dynamics onto that of a linear chain, it is shown that a localization-delocalization transition arises for a critical value of the generation number $G_c \approx 5$. This transition originates in the quantum interferences experienced by the excitonic wave due to the multiple scatterings that arise each time the wave tunnels from one generation to another. These results suggest that only small-size dendrimers could be used for designing an efficient quantum communication protocol.

PACS numbers:

I. INTRODUCTION

Performing high-fidelity quantum-state transfer (QST) from one region to another is a fundamental task in quantum information processing. It is needed to ensure an ideal communication between the elements of a computer or between different computers[1]. During the last decade, special attention has been paid for describing QST in spin networks[2–14]. Indeed, spin based communication protocols are one of the best candidates for scalable computing for two main reasons[15]. First, spin excitations delocalize in lattices owing to the interactions that naturally arise between neighboring sites. QST is thus spontaneously achieved without any external manipulation. Second, no interfacing is required between the communication channels and the computers, both components involving spin degrees of freedom.

However, spin networks are not the only ones that can be used to promote QST. The wide variety of collective excitations in condensed matter provides many alternatives. Consequently, various solid-state based protocols have been proposed. Examples among many are arrays of quantum dots[16,17], optical lattices[18,19], trapped ions[20], conducting polymers[21], phonons in low-dimensional crystals[22,23] and vibrons in molecular nanowires[24–26]. In the present paper, we consider a new idea where QST is mediated by Frenkel excitons that propagate in a dendrimer.

A dendrimer is an engineered hyperbranched polymer whose self-similar geometry at nanoscale resembles to the fractal patterns that occur in the plant kingdom[27–30]. The molecule is formed by a central core to which several dendritic branches are attached. Each branch, called a dendron, consists of long chains of molecular units arranged in a hierarchical fashion. The dendron exhibits branching points where the chain splits into two or three chains, depending on the connectivity, increasing the generation number. The end of the dendron is occupied by the functional terminal groups that form the periphery of the dendrimer. As a result, the dendrimer exhibits a series of chemical shells whose flexibility, porosity and surface functionalization can be adapted to perform many applications[28].

Among these applications, special attention has been paid during the last fifteen years to exploit the formal resemblance between tree-like molecules and photosynthetic antenna. A dendrimer behaves as an artificial light-harvesting complex able to convert the energy of a radiation into a chemical fuel[31–49]. To proceed, the main idea consists in the functionalization of the terminal groups by chromophores that are responsible for light harvesting. The capture of light generates electronic excitons that propagate along the dendrons. They converge toward the core that contains either a fluorescent trap, a reaction center or a chemical sensor[50,51].

As pointed out recently[52–55], the previous scenario suggests that exciton-mediated QST in dendrimers could be a promising way for quantum information processing. To proceed, one can imagine a protocol in which the terminal groups play the role of the computer where the information is implemented. The central core is thus occupied by a second computer where the information is received, the communication between the two computers being mediated by excitons propagating along the dendrons. Of course, in such a protocol, different ingredients prevent the occurrence of a perfect QST when a realistic system is considered : the inherent dispersion of the excitonic wave[2], the quantum decoherence due to the coupling with phonons[56,57] or the localization induced by disorder[58]. In this paper, an additional hindering is identified when an extended dendrimer is used, that is a localization-delocalization transition that occurs when the size of the dendrimer exceeds a critical value.

The paper is organized as follows. In Sec. II, the extended dendrimers we consider are described and the exciton Hamiltonian is defined. Then, the time-dependent Schrödinger equation is established and it is shown that the exciton dynamics can be mapped onto that of a linear chain. This problem is solved numerically in Sec. III where a detailed analysis of the dynamics is performed.

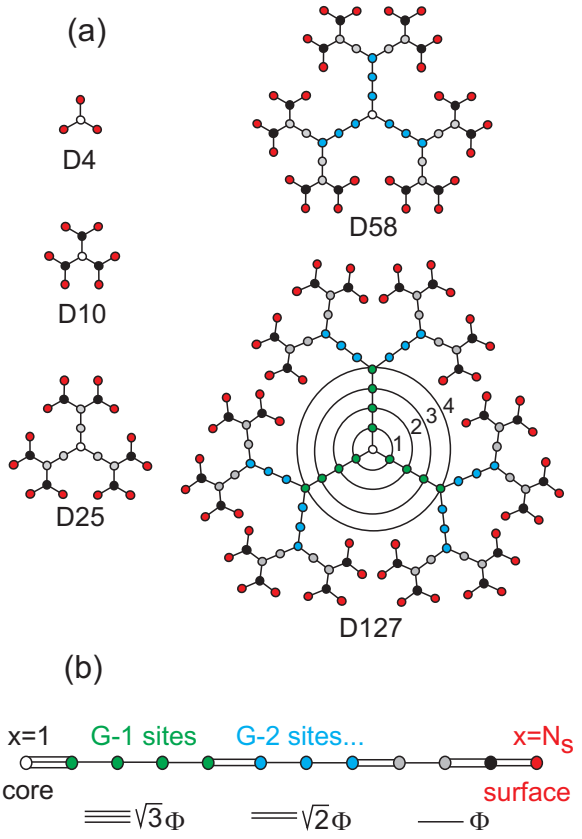

FIG. 1: (a) Poly-phenylacetylene extended dendrimers D4, D10, D25, D58 and D127. Each circle defines a phenyl ring whereas a connecting line stands for an acetylene group involving two single bonds and one triple bond. (b) Reduction of the exciton dynamics to a tight-binding model on a linear chain for $G = 5$ (see the text).

II. THEORETICAL BACKGROUND

A. Description of the dendrimer

As illustrated in Fig. 1a, we consider the family of the extended Poly-phenylacetylene dendrimers (PPA). Each dendrimer is built from linearly connected diphenylacetylene units that stand for molecular legs, and from phenyl rings that define branching points. The connectivity of the branching points being equal to three, each PPA has a threefold symmetry around its central core. It exhibits a fractal structure in which the length of the legs increases from the periphery to the core. Note that this contrasts with what happens in compact dendrimers where the bond length is the same between two branching points[34].

For describing the self-similar nature of an extended PPA, different ingredients are required[34]. First, one needs to specify the number of generations G that define the dendrimer. Then, the different generations are identified by the generation index $g = 0, 1, 2, ..., G$. The value $g = 0$ corresponds to the central core whereas $g = G$ refers to the $3 \times 2^{G-1}$ terminal groups. Otherwise, the value $g = 1, 2, ..., G-1$ describes the $3 \times 2^{g-1}(G-g)$ phenyl rings that belong to the gth generation. Each generation g is built from $G-g$ chemical shells labeled by the index $\ell_g = 1, ..., G-g$. Each shell contains equivalent phenyl rings that are symmetric to each other with respect to the rotational symmetry around the core. Therefore, $\ell_g = 1$ describes the $3 \times 2^{g-1}$ equivalent phenyl rings that belong to the first shell which surrounds the core. Similarly, $\ell_g = 2$ refers to the $3 \times 2^{g-1}$ equivalent phenyl rings that form the second shell which surrounds the first shell ... and so on. Note that the shell index is not required for describing the core site ($g = 0$) and the periphery ($g = G$). In both cases, it will be fixed to $\ell_0 = \ell_G = 1$. Finally, the total number of shells is equal to $N_s = 2 + G(G-1)/2$ and the total number of phenyl rings reduces to $N = 1 + 3 \times 2^{G-1} + 3 \times (2^G - G - 1)$.

To illustrate these features, Fig. 1a displays the five first PPA dendrimers D4, D10, D25, D58 and D127 for which the generation number G is successively equal to 1, 2, 3, 4 and 5. The number of phenyl rings varies from $N = 4$ to $N = 127$. Note that different colors have been used for describing the different generations. For instance, D127 involves $G = 5$ generations. The first generation (green circles) is formed by 12 phenyl rings organized into 4 shells (large circles) that surround the central core. Each shell involves 3 equivalent phenyl rings. The second generation (blue circles) involves 18 phenyl rings that are distributed into 3 shells (not drawn), each shell containing 6 equivalent phenyl rings. And so on until one reaches the periphery that corresponds to a single shell built with 48 equivalent phenyl rings (red circles).

B. Exciton Hamiltonian

According to the previous description, phenyl rings define sites for a lattice model that describes the dynamics of Frenkel excitons[31–38]. Therefore, each site $r = 1, ..., N$ is occupied by a two-level system that accounts for the electronic properties of a phenyl ring. Note that $r = 1$ refers to the core of the dendrimer. Let $|r\rangle$ stand for the first excited state of the rth two-level system and $\hbar\omega_0$ the corresponding energy. The set of orthogonal vectors $\{|r\rangle\}$ defines a local basis that entirely generates the one-exciton Hilbert space $\mathcal{E}$. Within this basis, the exciton dynamics is governed by a tight-binding Hamiltonian written as[31–38] (in unit $\hbar = 1$)

$$H = \sum_r \left(\omega_0 |r\rangle\langle r| + \sum_{r'} \Phi_{rr'} [|r\rangle\langle r'| + |r'\rangle\langle r|] \right), \quad (1)$$

where $\Phi_{rr'}$ is the exciton hopping matrix. It reduces to a constant Φ when r and r' correspond to nearest neighbor phenyl rings connected by a diphenylacetylene leg, otherwise it vanishes.

Note that we are aware of the simplicity of the present model. More elaborated approaches have been developed for studying the exciton dynamics such as the Husimi

cactus description of Mukamel and co-workers[39–43], the dipole-dipole interaction model of Nakano and co-workers[44–46] and the *ab initio* calculations carried out by Yamaguchi and co-workers[47,48]. However, we do not aim to provide a detailed description of the exciton properties. Instead, we present an academic work whose goal is to understand the influence of general features, such as the topology and the size of the dendrimer.

C. Quantum Dynamics

The exciton dynamics is governed by the time-dependent Schrödinger equation written as

$$i|\dot{\Psi}(t)\rangle = H|\Psi(t)\rangle, \tag{2}$$

where $|\Psi(t)\rangle$ is the exciton quantum state at time t. Eq.(2) can be solved easily by diagonalizing the system Hamiltonian Eq.(1), provided that the initial state $|\Psi(0)\rangle$ is known. In this paper, we are interested in the ability of the dendrimer to exchange a quantum information between its periphery and its core. Therefore, we consider the particular situation in which the initial state is uniformly distributed over the subspace $\mathcal{E}_G$ formed by the terminal groups, as

$$|\Psi(0)\rangle = \frac{1}{\sqrt{3\times 2^{G-1}}}\sum_{r\in\mathcal{E}_G}|r\rangle. \tag{3}$$

In that case, following procedures used for describing quantum graphs[52–55], the exciton dynamics can be mapped onto that of a linear chain. This surprising property arises because the geometry of the dendrimer provides to the Hamiltonian specific symmetries. As a result, when the initial state is uniformly distributed over the equivalent sites of a given shell, it remains uniformly distributed in each shell as time elapses. The dynamics is thus confined in a N_s dimensional subspace of the full Hilbert space that is spanned by N_s shell states. A shell state $|g,\ell_g\rangle$ is a uniform superimposition over the subspace $\mathcal{E}_{g,\ell_g}$ formed by the $3\times 2^{g-1}$ equivalent sites that belong to the ℓ_gth shell of the gth generation, as

$$|g,\ell_g\rangle = \frac{1}{\sqrt{3\times 2^{g-1}}}\sum_{r\in\mathcal{E}_{g,\ell_g}}|r\rangle. \tag{4}$$

Note that for $g=0$, the shell state $|0,1\rangle$ reduces to the core site $|r=1\rangle$.

Within the shell state basis, the Schrödinger equation is isomorphic to that of a fictitious particle that moves on a linear chain formed by N_s sites $x=1,...,N_s$. This linear chain is shown in Fig. 1b for $G=5$ and $N_s=12$. Each site x refers to a particular shell state $|g,\ell_g\rangle$. The site $x=1$ is associated to the core state $|g=0,\ell_0=1\rangle$. Then, the $G-1$ following sites $x=2,...,G$ are connected to the shell states of the first generation $|g=1,\ell_1\rangle$, with $\ell_1=1,...,G-1$. The $G-2$ following sites $x=G+1,...,2G-1$ refer to the shell states of the second generation $|g=2,\ell_2\rangle$, with $\ell_2=1,...,G-2$ ... And so on until one reaches the site $x=N_s$ that is related to the periphery of the dendrimer $|g=G,\ell_G=1\rangle$. Within this notation, the Schrödinger equation is finally expressed as

$$i\dot{\Psi}_x(t) = \omega_0\Psi_x(t) + \sum_x \Phi_{xx'}\Psi_{x'}(t), \tag{5}$$

where $\Psi_x(t)$ is the wave function of the fictitious particle on the xth site of the chain, that is the exciton wave function on any site belonging to the ℓ_gth shell of the gth generation that corresponds to the site x. Note that $\Psi_1(t)$ reduces to the wave function on the core site, i.e. the wave function whose knowledge is required for measuring the fidelity of the QST between the periphery and the core.

From Eq.(1), the non vanishing elements of the hopping matrix $\Phi_{xx'}$ are described as follows (see Fig. 1b). First, $\Phi_{xx'}=\Phi$ when x and $x'=x\pm 1$ are nearest neighbor sites on the chain that refer to nearest neighbor shells of the same generation. Then, $\Phi_{xx'}=\sqrt{2}\Phi$ when x and $x'=x\pm 1$ are nearest neighbor sites on the chain connected to nearest neighbor shells of neighboring generations. Finally, the hopping constant between the core and the first shell of the first generation is accounted by the parameter $\Phi_{12}=\Phi_{21}=\sqrt{3}\Phi$. In other words, when compared with a perfect chain with hopping constant Φ between neighboring sites, one obtains a perturbed chain which exhibits bond defects that are almost periodically distributed: $G-1$ bond defects $\sqrt{2}\Phi$ occur between the sites $x_g=1+gG-g(g+1)/2$ and x_g+1, with $g=1,...,G-1$, and one defect $\sqrt{3}\Phi$ arises between the sites $x=1$ and $x=2$. Note that this contrasts with what happens in compact dendrimers for which the corresponding chain is almost perfect, the hopping constant between nearest neighbors sites being equal $\sqrt{2}\Phi$. The chain only exhibits a bond defect $\sqrt{3}\Phi$ between the sites $x=1$ and $x=2$[52].

III. NUMERICAL RESULTS

In this section, the previous formalism is applied for describing QST between the periphery of the dendrimer and its central core. Within the equivalent linear chain model, this transfer characterizes the ability of the fictitious particle to propagate from one end of the chain to the other. The fidelity of the transfer is thus measured by the probability $P_1(t)=|\Psi_1(t)|^2$ to observed the particle on site $x=1$ at time t provided that it was located on site $x=N_s$ at time $t=0$.

The time evolution of $P_1(t)$ is illustrated in Fig. 2 for different generation numbers. As shown in Fig. 2a, when $G=1$ (black curve) and $G=2$ (red curve), $P_1(t)$ is a time periodic function whose period slightly increases with G. Note that similar features have been previously observed by Mulken et al.[52]. The period is equal to $1.81\Phi^{-1}$ for $G=1$ and it reaches $2.81\Phi^{-1}$ for $G=2$. The

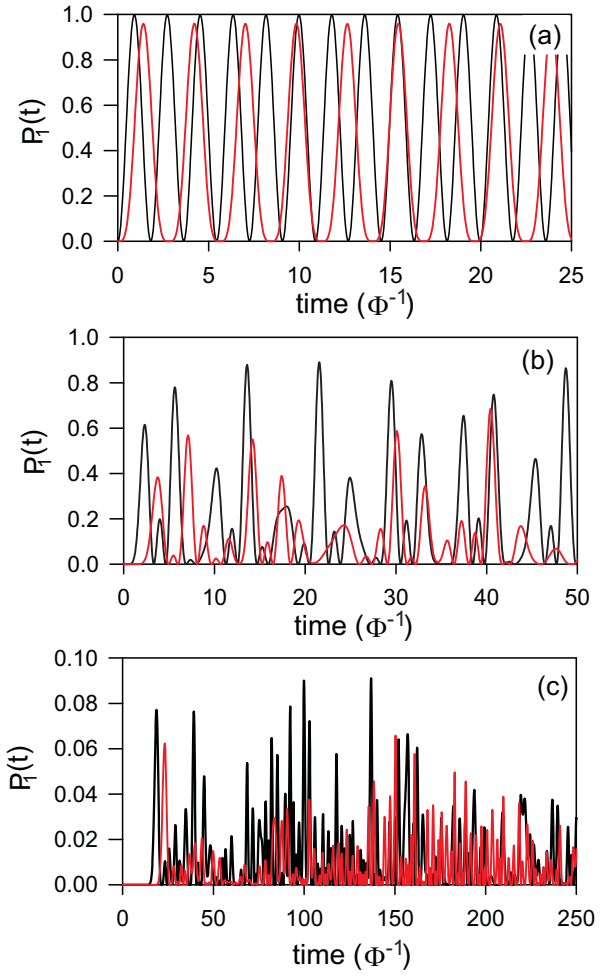

FIG. 2: Time evolution of the population of the core site $P_1(t)$ for different generation number G. (a) $G = 1$ (black curve) and $G = 2$ (red curve), (b) $G = 3$ (black curve) and $G = 4$ (red curve), (c) $G = 9$ (black curve) and $G = 10$ (red curve).

key point is that $P_1(t)$ ranges between zero and unity for $G = 1$ indicating that a perfect QST occurs in D4. By contrast, this is no longer the case for D10 ($G = 2$) because the maximum value of the core population reduces to $P_{max} = 0.96$. If one defines $P = 100 \times (1 - P_{max})$ as the percentage of lost information, one thus obtains $P = 4\%$.

As displayed in Fig. 2b, $P_1(t)$ no longer evolves periodically for $G = 3$ (black curve) and $G = 4$ (red curve). Instead, it becomes an almost time periodic function that exhibits more or less pronounced peaks. For $G = 3$, the almost period that separates two successive peaks is approximately $7.96\Phi^{-1}$. However, over a longer time scale, peaks whose amplitude is larger than 0.89 occur almost periodically, the corresponding periodic being approximately $35.10\Phi^{-1}$. These peaks describe quantum recurrences that arise because of the discreteness of the energy spectrum of the linear chain[59]. Consequently, owing to the presence of these recurrences, QST remains quite efficient in D25, the lost information being approximately

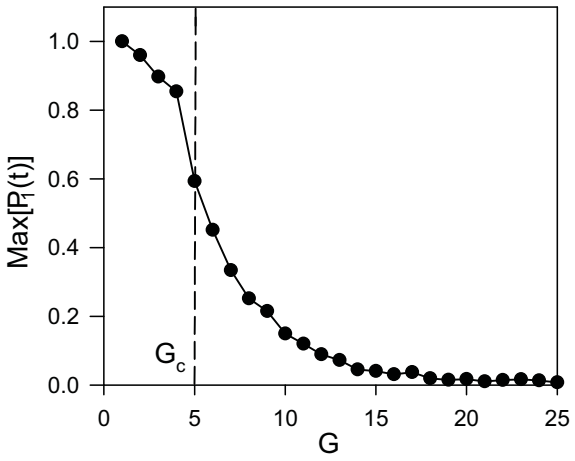

FIG. 3: Maximum value of the population $P_1(t)$ vs the generation number G. The simulation was carried out using 5×10^6 time steps over a time interval fixed to $5 \times 10^4\Phi^{-1}$.

10%. For $G = 4$ (D58), a similar behavior occurs but over different time scales. Indeed, quantum recurrences whose the amplitude is close to 0.84 were observed. But in that case, recurrences are very rare and they appear with a period of about $730\Phi^{-1}$ (not drawn). Note that the lost information is approximately 15%.

Finally, when the generation number increases, two main differences take place as displayed in Fig. 2c. First, the relevant time scales are now extremely long and second, the amplitudes of the quantum recurrences drastically decrease. For $G = 9$ (black curve), over a time scale equal to $1000\Phi^{-1}$, the first recurrence appears at $t = 971.26\Phi^{-1}$ and the corresponding amplitude is equal to 0.145 (not distinguishable on Fig. 2c). Similarly, for $G = 10$ (red curve), the first recurrence, whose amplitude is equal to 0.074, occurs at $t = 517.72\Phi^{-1}$. In that case, the lost information reaches 92%. In other words, when the number of shells that form the dendrimer becomes rather large, the maximum value of $P_1(t)$ deviates from unity resulting in the impoverishment of the transferred information.

The influence of the shell number is illustrated in Fig. 3 that shows the behavior of the maximum value P_{max} taken by the population of the core site with respect to the generation number G. Note that the simulation was carried out over a time scale fixed to $5 \times 10^4\Phi^{-1}$. The figure reveals the occurrence of a critical value $G_c \approx 5$ that discriminates between two regimes. When $G < G_c$, P_{max} varies almost linearly with G. It slightly decreases from unity for $G = 1$ to 0.84 for $G = 4$ so that the lost information remains smaller than 16%. By contrast, when $G \geq G_c$, a different behavior arises. P_{max} follows a decaying exponential function that scales as $P_{\max} = P_c \exp[-\alpha(G - G_c)]$, with $P_c \approx 0.59$ and $\alpha \approx 0.27$. Consequently, it drastically decreases with the generation number. Equal to 0.59 for $G = 5$, P_{max} reduces to 0.073 for $G = 13$. It reaches 0.008 for $G = 25$, a generation number for which the lost information is larger

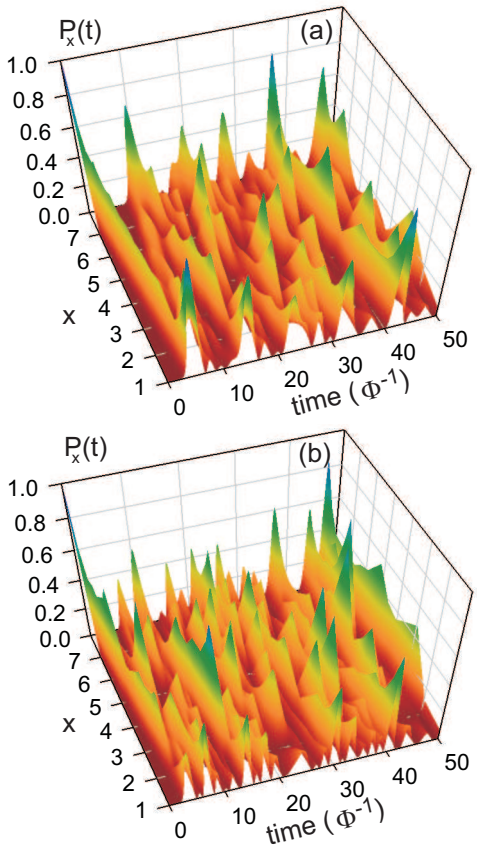

FIG. 4: Space time evolution of the probability density $P_x(t)$ (a) on the perfect chain and (b) on the perturbed chain for $G = 4$ and $N_s = 8$.

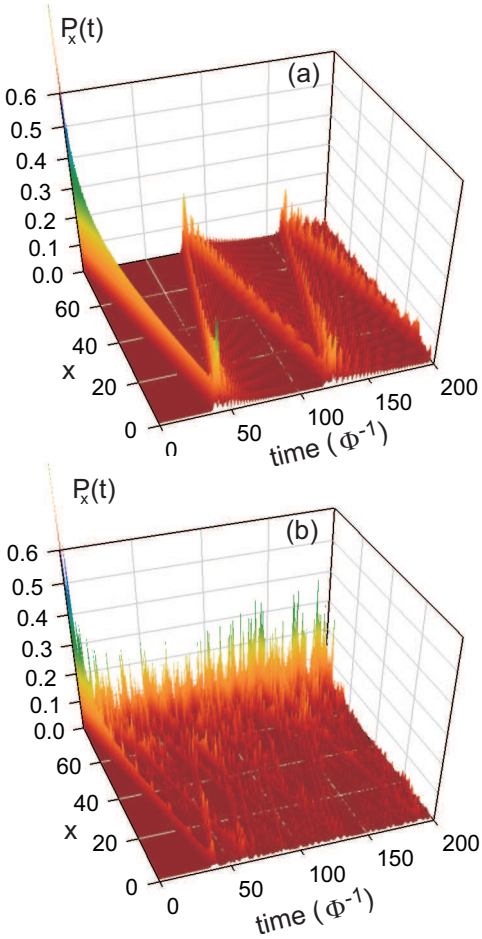

FIG. 5: Space time evolution of the probability density $P_x(t)$ (a) on the perfect chain and (b) on the perturbed chain for $G = 13$ and $N_s = 80$.

than 99%. Note that the time for which $P_1(t)$ reaches P_{max} strongly varies with G so that very different values have been observed. For instance, for $G = 7$, this time is equal to $2293.70\Phi^{-1}$. By contrast, for $G = 9$, it is approximately $48696\Phi^{-1}$ and it reaches $280340\Phi^{-1}$ for $G = 10$.

To clarify the difference between these two regimes, let us characterize the space time evolution of the probability $P_x(t) = |\Psi_x(t)|^2$ to observe the fictitious particle on site x at time t provided that it was initially on site $x = N_s$. Note that to understand the influence of the dendrimer topology, that is the influence of the bond defects that are distributed along the chain, we also consider the case of a perfect chain in which all the hopping constants are fixed to Φ. For $N_s = 8$, Fig. 4a reveals that in a perfect chain the fictitious particle behaves as a free wave packet that propagates between the two sides. First, a direct transfer arises so that $P_1(t)$ reaches a maximum value equal to 0.85 at $t = 5.05$. This transfer occurs according to a velocity equal to $v \approx 1.78\Phi$. Then, the wave packet is reflected and it realizes round-trips between the two sides. However, a fast spreading takes place owing to the strong dispersion. Consequently, the wave packet interferes with itself after each reflection resulting in the decay of $P_1(t)$ each time the wave packet recurs on the side $x = 1$. Nevertheless, because the confined particle exhibits a discrete energy spectrum, the dynamics is characterized by quantum recurrences. For instance, at $t = 42.20$, $P_1(t)$ is suddenly enhanced and it reaches 0.84. As illustrated in Fig. 4b, the fictitious particle behaves similarly in the perturbed chain. Nevertheless, few differences arise. First, the direct transfer is faster and the corresponding velocity is equal to $v \approx 2.40\Phi$. Therefore, $P_1(t)$ reaches a maximum value equal to 0.38 at $t = 3.75$. Then, the wave packet still realizes round-trips between the lattice sides. However, in addition to the reflections induced by the chain sides, the particle experiences scattering owing to the bond defects. As a result, a more complex self-interference pattern is drawn. Nevertheless, because of the reduced size of the chain, an efficient transfer arises owing to the occurrence of quantum recurrences. For instance, at $t = 40.45$, the population of the site $x = 1$ reaches 0.68.

When $G = 13$, that is for a longer chain involving $N_s = 80$ sites, the space time evolution of the density

probability is shown in Fig. 5. As displayed in Fig. 5a, the perfect chain still supports the propagation of a wave packet that experiences reflections on the lattice sides and whose amplitude decays owing to the lattice dispersion. A direct transfer arises at $t = 42.20$ for which $P_1(t)$ reaches 0.32. The corresponding velocity is approximately $v \approx 1.92\Phi$. Note that the self-interference pattern is clearly seen after each reflection on the lattice sides. As shown in Fig. 5b, a fully different behavior occurs in the perturbed chain and we do not recover a propagation phenomenon. Instead, the probability density resembles to a mountain range whose peaks draw a band in the 2D space time plot. Indeed, when one follows the direct propagation of the initial wave packet, one clearly distinguishes structures that account for intermediate reflections over the bond defects. These scatterings prevent the occurrence of an efficient direct transfer so that $P_1(t)$ reaches a maximum value equal to 0.03 at $t = 39.6$. Note that the corresponding velocity is approximately $v \approx 2.04\Phi$. In fact, the series of reflections favors the self-interference of the particle that tends to localize near the excited side of the perturbed chain. This localization arises over a length scale of about 15 sites starting from site $x = N_s$, that is the region where the probability density exhibits pronounced peaks. The average probability to observe the fictitious particle in the range $65 < x < 80$ is equal to 0.54.

Fig. 6 displays the time evolution of the expectation value of the position $\langle x(t)\rangle$ of the fictitious particle on the linear chain. Two generation numbers are used, that is $G = 4$ (Fig. 6a) and $G = 13$ (Fig. 6b), and always for the sake of comparison we consider the perfect chain (red curves) and the perturbed chain (black curves). Note that the simulation was carried out over a time scale equal to $2000\Phi^{-1}$. In a short perfect chain ($N_s = 8$), Fig. 6a shows that $\langle x(t)\rangle$ decreases from its initial value N_s until it reaches a minimum value equal to 1.5 at $t = 5.0\Phi^{-1}$. Then, it increases and it finally exhibits almost periodic oscillations around a stationary value $\bar{x} = 4.5$ exactly located at the center of the chain ($\bar{x} = (N_s + 1)/2$). In the perturbed chain, $\langle x(t)\rangle$ behaves similarly. It varies almost periodically and it oscillates around a stationary value $\bar{x} \approx 4.63$. In other words, for small N_s values, the particle behaves as a confined wave packet that delocalizes between the two sides of the chain.

In a longer chain ($N_s = 80$), a different behavior occurs as illustrated in Fig. 6b. Indeed, in the perfect chain, the particle sill performs round-trips between the two sides. Because the wave packet irreversibly spreads out, $\langle x(t)\rangle$ exhibits damped oscillations around the stationary value $\bar{x} = 40.50$ that still refers to the center of the chain. The corresponding period is approximately $80\Phi^{-1}$. By contrast, in the perturbed chain, $\langle x(t)\rangle$ decreases from its initially value N_s until it reaches a minimum value approximately equal to 50.0 at $t = 57.0\Phi^{-1}$. Then, it increases and it finally exhibits almost periodic oscillations around a stationary value $\bar{x} \approx 57.31$. The main period of these oscillations is approximately $160\Phi^{-1}$, that is

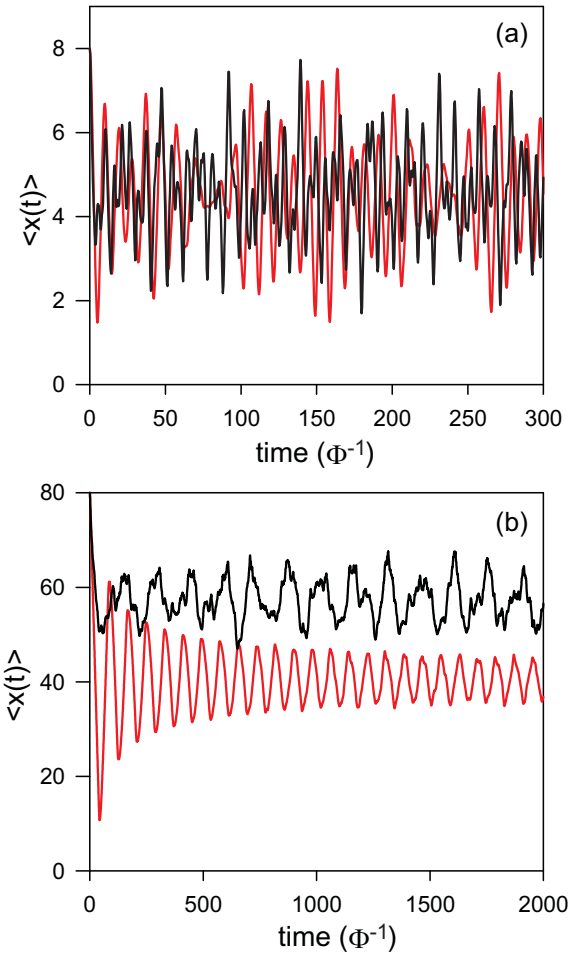

FIG. 6: Time evolution of the expectation value of the position of the fictitious particle for (a) $G = 4$ and (b) $G = 13$. Red curves correspond to the perfect chain whereas black curves refer to the perturbed chain.

twice the period of the oscillations observed in the perfect chain. The key point is that $\bar{x}$ deviates from the center of the chain and it gets closer to the excited edge $x = N_s$.

Fig. 7 generalizes the results displayed in Fig. 6 and shows the variation of the stationary value of the particle position $\bar{x}$ with respect to the generation number G. In the perfect chain (red curve), $\bar{x} \approx (N_s + 1)/2$, indicating that the probability density $P_x(t)$ delocalizes symmetrically around the center of the chain. In the perturbed chain (black curve), a critical value $G_c \approx 5$ discriminates between two regimes. When $G < G_c$, $\bar{x} \approx (N_s + 1)/2$ scales as in the perfect chain suggesting that the particle propagates freely. By contrast, when $G > G_c$, a different behavior occurs and $\bar{x}$ clearly deviates from the center of the chain. It approximately scales as $\bar{x} \approx 0.8(N_s + 1)$ and it gets closer to the excited edge of the chain.

The previous results reveal that when G exceeds the critical value G_c, the symmetry of the propagation is broken so that the particle tends to localize near the edge where it was created. According to the well-known An-

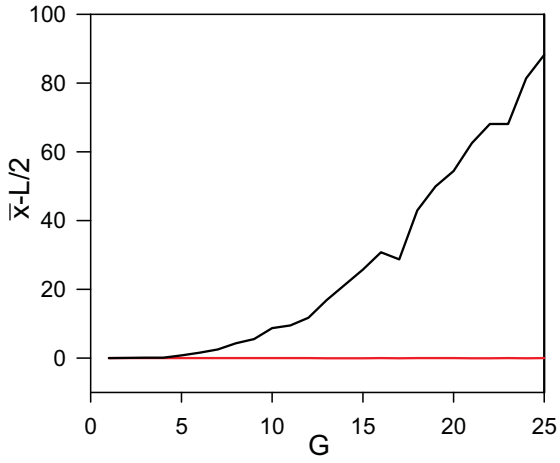

FIG. 7: Variation of the stationary value of the particle position $\bar{x}$ with respect to the generation number G in a perfect chain (red curve) and in a perturbed chain (black curve). Note that $L = (N_s + 1)$.

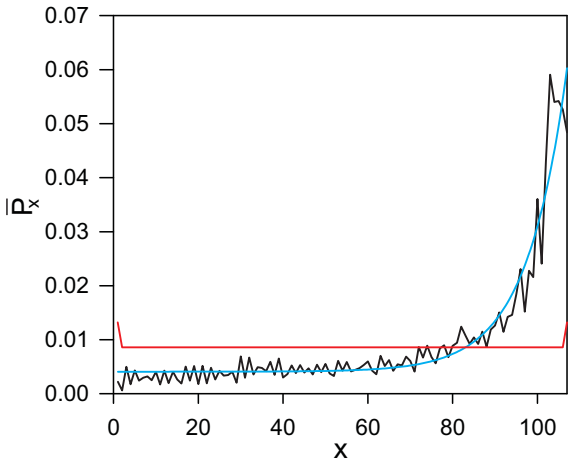

FIG. 8: Stationary distribution $\bar{P}_x$ vs x for $G = 15$ in a perfect chain (red curve) and in a perturbed chain (black curve). The blue curve defines the numerical fit discussed in the text.

derson theory[60], this phenomenon is characterized by the so-called localization length ξ that measures the typical length scale covered by the particle from $x = N_s$. To evaluate ξ, different approaches can be used, for instance, by studying the particle eigenstates or by calculating the inverse participation ratio. Here, we extract ξ from the x dependence of the stationary distribution $\bar{P}_x$ defined as

$$\bar{P}_x = \frac{1}{T}\int_0^T P_x(t)dt, \tag{6}$$

where the observation time T is sufficiently long to ensure the convergence. Such a definition arises because in a confined chain, the probability $P_x(t)$ is an almost periodic function of time. For each x value, it behaves as a random variable and it exhibits fluctuations around a stationary value that reduces to a time average.

Fig. 8 displays the behavior of the stationary distribution $\bar{P}_x$ vs x for $G = 15$. In a perfect chain (red curve), $\bar{P}_x$ is almost uniformly distributed indicating the occurrence of a delocalized phase. Over the sites $x \neq 1$ and $x \neq N_s$, it is equal to $\bar{P}_x = 1/(N_s + 1)$ whereas it becomes 1.5 times larger on the sites $x = 1$ and $x = N_s$. By contrast, in a perturbed chain (black curve), $\bar{P}_x$ is no longer symmetric with respect to the center of the chain and it no longer describes a quasi-uniform law. Instead, it is exponentially localized near the edge $x = N_s$ indicating that a localized phase occurs. As shown by the blue curve in Fig. 8, such a behavior is quite well captured by an exponential fit written as

$$\bar{P}_x = A + Be^{-(N_s - x)/\xi}, \tag{7}$$

where ξ stands for the localization length of the problem.

In that context, studying the curve $\bar{P}_x$ vs x for different generation numbers reveals that ξ follows a universal behavior (not drawn). It is almost independent on the generation number provides that $G > G_c$ and it is approximately equal to $\xi = 9.94 \pm 0.78$. Of course, when $G < G_c$, Eq.(7) no longer applies because of the extended nature of the stationary distribution (not drawn). Consequently, this constant value allows us to interpret the localization-delocalization as follows. When $\xi > N_s$, the particle is able to propagate from one end of the chain to the other resulting in a quite efficient QST. This is no longer the case when $\xi < N_s$ because the particle localizes before it reaches the site $x = 1$. The transition takes place when $\xi = N_s$. With $\xi = 9.94$ and provided that $N_s = 2 + G(G-1)/2$, one obtains $G_c \approx 4.52$, in a good agreement with the numerical results. Note that this transition is specific to extended dendrimers. It does not occur in compact dendrimers for which the corresponding linear chain does not exhibit bond defects.

IV. CONCLUSION

In this paper, exciton-mediated quantum state transfer between the periphery and the core of an extended dendrimer was investigated numerically. To proceed, we took advantage of the fact that the exciton dynamics can be mapped onto that of particle moving on a linear chain that exhibits bond defects. Within this equivalence, the fidelity of the transfer is measured by the ability of the particle to tunnel from one end of the chain to the other.

In that context, initially created on the site $x = N_s$, the particle behaves as a wave packet that propagates along the chain. This wave packet interacts with the bond defects that are quasi-periodically distributed. These interactions yield multiple scatterings at the origin of the wave packet self-interference. Therefore, these severe quantum interferences can completely halt the particle that tends to localize over a length scale given by the localization length $\xi \approx 9.94$. As a result, two situations arise. When $\xi > N_s$, the particle can reach the site $x = 1$ so that QST occurs with a rather important fidelity. By contrast, when $\xi < N_s$, the particle localizes before it

reaches the site $x = 1$ preventing any significant QST. The transition takes place when $\xi = N_s$, that is when the generation number reduces to $G_c \approx 5$.

In other words, in the original point of view, an excitonic wave that propagates from the periphery to the core of an extended dendrimer is prone to a localization-delocalization transition. This transition results from quantum interferences experienced by the excitonic wave owing to the multiple scatterings that occur each time the wave tunnels from one generation to another. Consequently, these results suggest that only the small-size dendrimers D4, D10, D25 and D58 can be used for designing an efficient quantum communication protocol. Of course, additional studies are required to check the influence of other phenomena that could potentially affect the fidelity of the transfer.

---

* Electronic address: vincent.pouthier@univ-fcomte.fr

[1] C.H. Bennet and D.P. DiVincenzo, Nature (London) **404**, 247 (2000).
[2] S. Bose, Phys. Rev. Lett. **91**, 207901 (2003).
[3] M. Christandl, N. Datta, A. Ekert, and A. J. Landahl, Phys. Rev. Lett. **92**, 187902 (2004).
[4] A. Ashok and P. Cappellaro, Phys. Rev. A **85**, 042305 (2012).
[5] D. Burgarth and S. Bose, Phys. Rev. A **71**, 052315 (2005).
[6] A. Wojcik, T. Luczak, P. Kurzynski, A. Grudka, T. Gdala, and M. Bednarska, Phys. Rev. A **72**, 034303 (2005).
[7] L. Campos Venuti, C. Degli Esposti Boschi, and M. Roncaglia, Phys. Rev. Lett. **99**, 060401 (2007).
[8] L. Banchi, T.J.G. Apollaro, A. Cuccoli, R. Vaia, and P. Verrucchi, Phys. Rev. A **82**, 052321 (2010).
[9] N.Y. Yao, L. Jiang, A.V. Gorshkov, Z.X. Gong, A. Zhai, L.M. Duan, and M.D. Lukin, Phys. Rev. Lett. **106**, 040505 (2011).
[10] Y. Li, T. Shi, B. Chen, Z. Song, and C.-P. Sun, Phys. Rev. A **71**, 022301 (2005).
[11] P. Karbach and J. Stolze, Phys. Rev. A **72**, 030301(R) (2005).
[12] M.H. Yung and S. Bose, Phys. Rev. A **71**, 032310 (2005).
[13] M.L. Hu and H.L. Lian, Eur. Phys. J. D **55**, 711 (2009).
[14] P. Cappellaro, L. Viola, and C. Ramanathan, Phys. Rev. A **83**, 032304 (2011).
[15] D. Burgarth, Eur. Phys. J. Special Topics **151**, 147-155 (2007).
[16] D. Loss and D.P. DiVincenzo, Phys. Rev. A **57**, 120 (1998).
[17] F.L. Semio, K. Furuya, and G.J. Milburn New J. Phys. **12**, 083033 (2010).
[18] O. Mandel, M. Greiner, A. Widera, T. Rom, T.W. Hansch, and I. Bloch, Nature (London) **425**, 937 (2003).
[19] J. Reslen and S. Bose, Phys. Rev. A **80**, 012330 (2009).
[20] H. Haffner, C.F. Roos, and R. Blatt, Phys. Rep. **469**, 155 (2008).
[21] M.X. Huo, Y. Li, Z. Song, and C.P. Sun, Eur. Phys. Lett. **84**, 30004 (2008).
[22] M.B. Plenio and F.L. Semio New J. Phys. **7** 73, (2005).
[23] M.B. Plenio, J. Hartley and J. Eisert, New J. Phys. **6**, 36 (2004).
[24] V. Pouthier, Phys. Rev. B **85**, 214303 (2012).
[25] V. Pouthier, J. Phys. Condens. Matter **24**, 445401 (2012).
[26] V. Pouthier, J. Chem. Phys. **139**, 054103 (2013).
[27] F. Vogtle, G. Richardt, and N. Werner, *Dendrimer Chemistry: Concepts, Syntheses, Properties, Applications* (Wiley, Weinheim, 2009).
[28] D. Astruc, E. Boisselier, and C. Ornelas, Chem. Rev. **110**, 1857 (2010).
[29] J.M.J. Frechet, Science **263**, 1710 (1994).
[30] A.W. Bosman, H.M. Janssen, and E.W. Meijer, Chem. Rev. **99**, 1665 (1999).
[31] K. Harigaya, Chem. Phys. Lett. **300**, 33 (1999).
[32] K. Harigaya, Phys. Chem. Chem. Phys. **1**, 1687 (1999).
[33] K. Harigaya, Int. J. Mod. Phys. B **13**, 2531 (1999).
[34] M.A. Martin-Delgado, J. Rodriguez-Laguna, and G. Sierra, Phys. Rev. B **65**, 155116 (2002).
[35] C. Supritz, A. Engelmann, and P. Reineker, J. Lumin. **111, 367** (2005).
[36] C. Supritz, A. Engelmann, and P. Reineker, J. Lumin. **119-120**, 337 (2006).
[37] C. Supritz, A. Engelmann, and P. Reineker, J. Lumin. **122-123**, 759 (2007).
[38] C. Supritz, V. Gounaris, and P. Reineker, J. Lumin. **128**, 877 (2008).
[39] S. Tretiak, V. Chernyak, and S. Mukamel, J. Phys. Chem. B **102**, 3310 (1998).
[40] E.Y. Poliakov, V. Chernyak, S. Tretiak, and S. Mukamel, J. Chem. Phys. **110**, 8161 (1999).
[41] V. Chernyak, E. Y. Poliakov, S. Tretiak, and S. Mukamel, J. Chem. Phys. **111**, 4158 (1999).
[42] T. Minami, S. Tretiak, V. Chernyak, and S. Mukamel, J. Lumin. **87-89**, 115 (2000).
[43] J.C. Kirwood, C. Scheurer, V. Chernyak, and S. Mukamel, J. Chem. Phys. **114**, 2419 (2001).
[44] M. Nakano, M. Takahata, H. Fujita, S. Kiribayashi, and K. Yamaguchi, Chem. Phys. Lett. **323**, 249 (2000).
[45] M. Nakano, M. Takahata, H. Fujita, S. Kiribayashi, and K. Yamaguchi, J. Phys. Chem. A **105**, 5473 (2001).
[46] M. Takahata, M. Nakano, H. Fujita, and K. Yamaguchi, Chem. Phys. Lett. **363**, 422 (2002).
[47] M. Nakano, M. Takahata, S. Yamada, K. Yamaguchi, R. Kishi, and T. Nitta, J. Chem. Phys. **120**, 2359 (2004).
[48] M. Nakano, R. Kishi, T. Minami, and K. Yoneeda, Molecules **14**, 3700 (2009).
[49] G.W. Crabtree and N.S. Lewis, Phys. Today **60**, 37 (2007).
[50] A. Bar-Haim, J. Klafter, and R. Kopelman, J. Am. Chem. Soc. **119**, 6197 (1997).
[51] M.S. Choi, T. Aida, T. Yamazaki, and I. Yamazaki, Chem. Eur. J. **8**, 2667 (2002).
[52] O. Mulken, V. Bierbaum, and A. Blumen, J. Chem. Phys. **124**, 124905 (2006).
[53] E. Agliari, A. Blumen and O. Mulken, Phys. Rev. A **82**, 012305 (2010).
[54] O. Mulken and A. Blumen, Phys. Rep. **502**, 37 (2011).
[55] A.M. Childs, E. Farhi, and S. Gutmann, Quantum Information Processing **1**, 35 (2002).
[56] V. Pouthier, J. Chem. Phys. **134**, 114516 (2011).
[57] V. Pouthier, Phys. Rev. B **83**, 085418 (2011).
[58] S. R. Jackson, T.J. Khoo, and F.W. Strauch, Phys. Rev. A **86**, 022335 (2012).
[59] V. Pouthier, Phys. Rev. E **81**, 031913 (2010).

[60] B. Kramer and A. MacKinnon, Rep. Prog. Phys. **56**, 1469 (1993).